Theoretical study of the effects of F to Cl chemical substitution on the electronic structure and the luminescence properties of $Cs_2GeF_6:Os^{4+}$ and $Cs_2ZrCl_6:Os^{4+}$ materials

José Luis Pascual[a)]
Departamento de Química Física Aplicada, C-14, Universidad Autónoma de Madrid, 28049 Madrid, Spain

Zoila Barandiarán and Luis Seijo
Departamento de Química, C-14 and Instituto Universitario de Ciencia de Materiales Nicolás Cabrera, Universidad Autónoma de Madrid, 28049 Madrid, Spain

(Received 21 July 2005; accepted 3 February 2006; published online 28 March 2006)

It has been experimentally determined that $Cs_2ZrCl_6:Os^{4+}$ shows luminescence and up-converted luminescence from the highest t_{2g}^4 excited level $2A_{1g}(^1A_{1g})$, whereas $Cs_2GeF_6:Os^{4+}$ $2A_{1g}(^1A_{1g})$ does not luminescence at all. *Ab initio* quantum chemical calculations on these materials are presented here and show that the variation of the energy gap between the t_{2g}^4 and $t_{2g}^3 e_g^1$ manifolds with F to Cl chemical substitution is a key factor to interpret the experimental findings. This energy gap is calculated to be some 1500 cm^{-1} ($\simeq 2\bar{\nu}_{a_{1g}}$) in the fluoride host, whereas it is about 3300 cm^{-1} ($\simeq 9\bar{\nu}_{a_{1g}}$) in the chloride host. The calculated values for the ground state totally symmetric vibrational frequency $\bar{\nu}_{a_{1g}}$ are 626 cm^{-1} ($Cs_2GeF_6:Os^{4+}$) and 355 cm^{-1} ($Cs_2ZrCl_6:Os^{4+}$), in good agreement with the available experimental data. Geometrical structure of $(OsX_6)^{2-}$ clusters (X=F,Cl) embedded in Cs_2GeF_6 and Cs_2ZrCl_6 lattices is calculated as well. New assignments for some spectral features based in the results of our calculations are proposed. © *2006 American Institute of Physics*. [DOI: 10.1063/1.2180772]

I. INTRODUCTION

Luminiscent materials are the subject of an increasing interest among the scientific community due to their technological applications, such as display screens, lamps, and solid state lasers. Special attention is being dedicated to materials which are able to convert long-wavelength radiation into a more energetic one, mainly through up conversion (UC) mechanisms (see, e.g., Ref. 1 and references therein). Up conversion is based on the existence of several metastable excited states in the material, and, due to this fact, ionic lattices doped with rare-earth elements are natural candidates to show up conversion. In fact, a number of this kind of systems have been studied and characterized over the last decades.[1] Although less numerous, some transition-metal doped materials have been shown to produce UC during the last years. For example, Gamelin and Güdel have described systems with Ni^{2+}, Ti^{2+}, Mo^{3+}, Re^{4+}, and Os^{4+} as dopants.[1] Varying chemical conditions can be induced by using different hosts for the ions, and this effect is reflected in the different behavior towards UC, so that new materials with the desired properties can be "tailored" by changing the ion's environment.

In this work we will focus on the properties of two Os^{4+}-doped ionic halides, namely, Cs_2GeF_6 and Cs_2ZrCl_6. Both systems have been experimentally investigated recently in relation to their UC properties, together with the related bromide compound, Cs_2ZrBr_6.[2–7] Significant UC is found for the doped chloride, with different characteristics depending on the exciting energy, but no UC is found for the fluoride. The optical spectrum and magnetic circular dichroism spectrum of $Os^{4+}:Cs_2ZrCl_6$ have been studied in the past[8–11] and the $(OsCl_6)^{2-}$ chromophore has been studied in other lattices as well[12–18] and in solution,[19,20] but the studies on the spectrum of $(OsF_6)^{2-}$ are less numerous.[7,13,21] Both Cs_2GeF_6 and Cs_2ZrCl_6 are cubic crystals, with the potassium chloroplatinate structure[22] and the dopant Os^{4+} ion which substitutes for a tetravalent cation (Ge^{4+} or Zr^{4+}), in a perfect octahedral coordination. Free Os^{4+} has the $5d^4$ electronic structure and in octahedral coordination, even in halide compounds, promotes a large ligand field splitting, so that the $^3T_{1g}(t_{2g}^4)$ state becomes the ground state, being followed in energy by predominantly spin singlet t_{2g}^4 levels. Some of these higher t_{2g}^4 excited states are metastable, a necessary premise for UC, and so, these levels are considered to be responsible for the transitions that lead to UC in $Os^{4+}:Cs_2ZrCl_6$[2,6] [also in the bromide doped analog $Os^{4+}:Cs_2ZrBr_6$ (Ref. 3)]. However, the luminescence that is involved in UC for these materials is not found in the fluoride compound[7] and the explanations given in the literature are related to the relative position of $t_{2g}^3 e_g^1$ levels (either the ^5E_g states[7] or the lowest lying triplet states[5]) with respect to the t_{2g}^4 manifold. The electronic transitions between all these states are electric dipole forbidden (g-g transitions), so their intensity should be small. In addition, the $t_{2g}^4 \rightarrow t_{2g}^3 e_g^1$ excitations are expected to be broad due to their interconfigurational character. Consequently, they can neither be resolved nor assigned in the spectrum and

[a)]Electronic mail: joseluis.pascual@uam.es

their position has to be inferred from ligand field calculations in which the parameters carry large uncertainties, especially the $10Dq$ parameter.

In view of these arguments, the question about the mechanism responsible for the different behavior towards UC in the two hosts is still open. In this paper, we present a theoretical investigation of these systems. The calculations show that all intraconfigurational transitions ($t_{2g}^4 \rightarrow t_{2g}^4$) are lower in energy than interconfigurational ($t_{2g}^4 \rightarrow t_{2g}^3 e_g^1$) transitions. We have also investigated the variation of the energy gap between the two manifolds with F to Cl chemical substitution and we find that this gap is smaller for the fluoride, around 1500 cm^{-1}, than for the chloride, around 3300 cm^{-1}. This difference is a crucial point to interpret the experimental results.

We have structured the paper as follows: In Sec. II we present a brief overview of the method together with the details of the calculations. In Sec. III we present the results of the calculations performed on the Os^{4+} free ion, which give useful information for the embedded cluster calculations, and in Sec. IV we present the results of the cluster calculations with a comparison with the available experimental information. We discuss some aspects of the results in Sec. V, and the conclusions are presented in Sec. VI.

II. METHOD AND DETAILS OF THE CALCULATIONS

A. Embedding potentials

The optical spectrum of the defect center formed when an Os^{4+} ion substitutes for a tetravalent cation (Ge^{4+} or Zr^{4+}) in ionic compounds such as Cs_2GeF_6 and Cs_2ZrCl_6 corresponds to electronic transitions localized in the $(OsX_6)^{2-}$ (X=F,Cl) cluster unit, and is supposed to be governed by the bonding interactions between the impurity Os^{4+} and the first neighbor halide anions. These interactions can be adequately described by applying standard high quality quantum mechanical methods to the $(OsX_6)^{2-}$ cluster. The embedding effect due to interactions of the cluster atoms with the rest of the components of the host lattice is also important. In this work, we model it by using the *ab initio* model potential (AIMP) embedding technique.

This AIMP embedding technique is a practical implementation to the study of local properties of imperfect solids of the group function theory developed by McWeeny,[23] in the context of intermolecular interactions, and Huzinaga,[24] in the context of core/valence partition. It has been presented in Refs. 25 and 26 as a technique to perform calculations on perfect, unpolarized ionic lattices, and later extended[27] to allow for calculations with a relaxed and polarized lattice, represented by a shell-model description.[28] Its application to impurity defects has been reviewed in Ref. 29. In practice, an embedding potential is added to the one-electron Hamiltonian of the free cluster. This potential consists of a sum over the lattice ions of total-ion potentials of the form

$$V_\mu^{\mathrm{lr\ Coul}}(i) + V_\mu^{\mathrm{sr\ Coul}}(i) + V_\mu^{\mathrm{exch}}(i) + P_\mu(i), \qquad (1)$$

where μ labels the lattice ions (Cs^+, Ge^{4+}, and F^- in Cs_2GeF_6; Cs^+, Zr^{4+}, and Cl^- in Cs_2ZrCl_6); $V_\mu^{\mathrm{lr\ Coul}}(i)$ stands for the long-range Coulomb potential exerted by ion μ on the ith electron of the cluster (i.e., $\Sigma_\mu V_\mu^{\mathrm{lr\ Coul}}(i)$ is the Madelung potential of the lattice); $V_\mu^{\mathrm{sr\ Coul}}(i)$ stands for the potential that represents the deviation from point-charge character of the lattice ion (the short-range Coulomb potential); $V_\mu^{\mathrm{exch}}(i)$ is the exchange potential, which stems from the fact that the wave function of the whole system (cluster plus lattice) has to be antisymmetric with respect to the interchange of electrons between the cluster and the lattice group functions; $P_\mu(i)$ is the orthogonality operator that prevents the cluster wave function from collapsing onto the lattice ion μ. The embedding potentials used in this work were obtained in calculations of structural and spectral properties of Mn^{4+}-doped Cs_2GeF_6 (Ref. 30) and Pa^{4+}-doped Cs_2ZrCl_6.[31] For the details concerning their obtention, we refer to the original papers.

The AIMP embedding potential is, ideally, built up by adding to the cluster Hamiltonian the AIMP total-ion potentials of all the lattice ions outside the cluster. In practice, the infinite sum is truncated, in such a way that we include the AIMP embedding potentials of all ions located within the cube of length $2a$ centered in the impurity site (a=9.021 Å for the fluoride and a=10.407 Å for the chloride; a total of 420 ions) plus all ions located outside this cube but inside the cube of length $4a$, (2394 ions more) these ones as point charges bearing the nominal ion charge, except those located at the frontier, which bear fractional charges according to Evjen's method.[32] In this way we can be sure that the cluster embedding potential provides a good representation of the quantum effects as well as the long-range Madelung effects.

B. Defect cluster calculations

As stated above, in order to obtain good agreement with the observed properties, the calculations performed on the defect clusters $(OsX_6)^{2-}$ (X=F,Cl) should include nondynamic as well as dynamic electron correlation and relativistic effects, including spin-orbit coupling. A natural way to fulfill this requirements is to perform multireference spin-orbit configuration interaction (CI) calculations on the clusters. However, the number of valence electrons that should be correlated to obtain good quality in the results is quite large, a total of 60 (12 from the Os^{4+} ion and 48 from the ligands), as it has been shown[33,34] that for intermediate oxidation states of the impurities (such as the IV oxidation state of Os in these systems) the use of CI expansions that include only a subset of the ligand p electrons could result in large discrepancies with experimental results. For such a high number of correlated electrons, the above mentioned multireference spin-orbit CI calculations will be too costly from the computational point of view. Then, we will treat these effects by an approximate procedure, the spin-free-state-shifted (ssfs) relativistic Hamiltonian,[34] which can decouple electron correlation and spin-orbit effects in a very efficient way. This method is a two-step procedure: in a first step, spin-free Hamiltonian calculations are performed, in which scalar relativistic effects and electron correlation are dealt with at the highest methodological level possible. In the second step, the effect of electron correlation upon the transition energies is transported by the sfss operator to spin-orbit CI calculations

performed in a CI space smaller than the corresponding spin-free one. This procedure has been successfully applied to transition-metal[34] and *f*-element impurities.[30,35–37]

We will start by describing the spin-free calculations. First, we have performed complete active space self-consistent field[38] (CASSCF) calculations, including four active electrons in the mainly Os^{4+} $5d$ molecular orbitals. The wave functions were optimized, at this level, for averages of different states, according to their spin and spatial symmetry. Four different state averaged optimizations were performed, namely, for the states of symmetry $\langle {}^1A_{1g}, {}^1A_{2g}, {}^1E_g\rangle$, $\langle {}^1T_{1g}, {}^1T_{2g}\rangle$, $\langle {}^3A_{1g}, {}^3A_{2g}, {}^3E_g\rangle$, and $\langle {}^3T_{1g}, {}^3T_{2g}\rangle$. The excited ${}^5E_g$ state was treated in a separate optimization. We have optimized all the states coming from the t_{2g}^4 and $t_{2g}^3e_g^1$ electron configurations. To include dynamic electron correlation, we have performed calculations using an extension of the second order multiconfigurational perturbation method CASPT2 (Ref. 39) and the multistate CASPT2 method.[40,41] The CASSCF wave functions were used as a multidimensional zeroth order wave function for the perturbation treatment. A total of 60 electrons were correlated, those occupying the molecular orbitals of main character Os $5s$, $5p$, $5d$ and F $2s$, $2p$ (for the fluoride compound) or Cl $3s$, $3p$ (for the chloride). For all the distances studied in this work, the preliminary single-state CASPT2 calculations showed good behavior: large and uniform weight of the zeroth order wave function and no sign of intruder states. This weight was found to be larger in the fluoride (>70%) than in the chloride (>60%). The only exception to this behavior is the $2\,{}^1A_{1g}$ state of the $(OsCl_6)^{2-}$ cluster, which has a weight of the zeroth order wave function of the order of 50% for the larger distances that we have considered.

We have performed all the spin-free calculations using relativistic core AIMPs and valence basis sets. For the Os atom, a relativistic core AIMP for the $[Cd,4f]$ core has been published,[42] based on Cowan-Griffin-Wood-Boring[43,44] calculations together with the corresponding valence basis sets and Wood-Boring spin-orbit operators. However, it has been shown that, for lanthanide and actinide elements, the transferability of the core AIMPs between the neutral atoms and its ions is not guaranteed for relatively large cores.[30,36] There, it was also shown that the use of a smaller [Kr] core provides an accurate description of spin-orbit coupling constants and transition energies both for the neutral atom and the ions.[36] Following these works, we have produced a relativistic [Kr]-core AIMP, mass-velocity, and Darwin operators and optimized a valence basis set for the Os atom in its ${}^5D$ ground state $(5d^6,6s^2)$. The valence consists of the $4d4f5s5p5d6s$ orbitals for the neutral atom, and the potentials are expected to be transferable to the Os^{4+} ion reliably. The potentials have been obtained following the same recipes used in Ref. 42, except that the analytical representation of the core orbitals has been obtained by maximizing the overlap with the numerical core orbitals *and* imposing restrictions of orthogonality to the valence numerical orbitals. The *p* block of the basis set has been spin-orbit corrected in the usual way.[45] The valence basis set $(15s10p10d8f)$ was augmented with a *p*-type polarization function[46] and a *d* diffuse function, the same with that used in Ref. 42, and was finally contracted to $[6s5p6d4f]$ in the cluster calculations. We have investigated the effect of the inclusion of *g* functions in the basis set of Os in a series of calculations of the spectroscopic parameters of the $(OsCl_6)^{2-}$ cluster and found that the effects were negligible for the geometry and electronic transitions.

For fluorine, we have used a [He] core and primitive basis set taken from Ref. 47; the $(5s5p)$ set of primitives, augmented by one diffuse *p* for anions optimized for fluoride crystals in $KMgF_3:F^-$ embedded cluster calculations[48] and $1d$ polarization function,[46] was contracted to $[2s3p1d]$. For chlorine, we have used a [Ne]-core relativistic Cowan-Griffin-Wood-Boring AIMP and valence basis set $(7s6p)$, taken from Ref. 49 augmented by $1p$ diffuse anion function[50] and $1d$ polarization function,[46] with the final contraction being $[3s4p1d]$. The total numbers of basis functions 175 for the fluoride and 199 for the chloride. AIMP potentials (both core and embedding) and basis sets are available in electronic format from the authors.[51]

All the Cowan-Griffin relativistic spin-free calculations just described have been performed using the MOLCAS (Ref. 52) program system.

As stated above, once the potential energy curves for the states of interest have been calculated at the MS-CASPT2 level, the dynamic correlation effects can be transported to the spin-orbit CI calculations to be performed in a smaller configurational space through the spin-free-state-shifted Wood-Boring (WB) AIMP Hamiltonian.[29,34,45] This Hamiltonian results from adding to the many-electron spin-orbit WB-AIMP Hamiltonian[45] the so-called spin-free state shifting operator:

$$\sum_{iSM_S\Gamma\gamma} \delta(iS\Gamma)|\Phi^{\mathcal{P}}(iSM_S\Gamma\gamma)\rangle\langle\Phi^{\mathcal{P}}(iSM_S\Gamma\gamma)|, \tag{2}$$

where $\delta(iS\Gamma)=\Delta E^{\mathcal{G}}(iS\Gamma)-\Delta E^{\mathcal{P}}(iS\Gamma)$. Here, $\Delta E^{\mathcal{G}}(iS\Gamma)$ is the transition energy (with respect to the $1\,{}^3T_{1g}$ ground state of the cluster) of the different $iS\Gamma$ spin-free excited states at the MS-CASPT2 level. $\Delta E^{\mathcal{P}}(iS\Gamma)$ is the transition energy for the same state, but computed in the smaller CI space. Then, the effect of the operator is to shift the spin-free states calculated in a small CI space (space $\mathcal{P}$) to the position of the same states calculated in the large CI space (space $\mathcal{G}$). In this case, $\mathcal{P}$ is the CI space defined by the complete Os $5d^4$ active space plus all the single excitations to the virtual space.

The spin-orbit part of the WB-AIMP Hamiltonian is defined as a sum of atomic one-electron spin-orbit (SO) terms $\hat{h}_{\mathrm{SO}}^I(i)$ (Ref. 45),

$$\hat{h}_{\mathrm{SO}}^I(i) = \lambda^I \sum_{n\ell} V_{\mathrm{SO}n\ell}^{I,MP}(r_i)\hat{\mathcal{O}}_\ell^I \hat{l}^I \hat{s} \hat{\mathcal{O}}_\ell^I, \tag{3}$$

where I labels the different cluster ions (I=Os for the fluoride; I=Os, Cl for the chloride). This term has been describe in detail elsewhere,[29,30,45] here we will only stress the point that the parameter λ^I may act as a scaling factor for the spin-orbit contribution of atom I. We will make use of this fact later. For this spin-orbit CI calculations, the one-electron basis sets used were the same with that described above. The calculations were performed using molecular orbitals optimized in an average of the $\langle {}^1A_{1g}, {}^1A_{2g}, {}^1E_g\rangle$ states.

The spin orbit calculations presented in this work were performed using a modified version of the COLUMBUS suite of programs.[53] All the calculations that we present in subsequent sections have been performed at this ssfs WB-AIMP MS-CASPT2 level of theory, unless otherwise indicated.

III. THE ABSORPTION SPECTRUM OF GAS PHASE Os^{4+}

In theoretical studies of impurities in ionic hosts, it is costumary to perform a preliminary calculation of the spectra of the doping ion in the gas phase because it can help in establishing the quality of the different "ingredients" (basis set, spin-orbit operator, and electron correlation) of the method at the atomic level. (See examples in Ref. 29). To this end, we have calculated the *d-d* spectrum of the gas phase Os^{4+} ion at the sfss spin-orbit level. The basis set for Os was that described in the preceeding section. We performed spin-free MS-CASPT2 calculations including 12 valence electrons $(5s,5p,5d)$ and then spin-orbit CI (single excitations) using the sfss Hamiltonian. In this analysis we will focus on the lower portion of the spectrum (i.e., below 50 000 cm^{-1}), especially in the spin-free ^5D, $1\,^3P$, $1\,^3F$, ^3D, ^3H, ^3G, $1\,^1D$, ^1F, ^1I, and $1\,^1G$ states. We focus on these states because the spin-free states of the clusters that will be of interest to us (the t_{2g}^4 and $t_{2g}^3e_g^1$ manifolds) are related to these atomic spin-free states. We present the results of such calculations and a comparison with the available experimental results in Table I and in Fig. 1.

The second column on the table shows the results we have just described (ordered by increasing energy within the manifold of a given J value). The comparison of these results with experimental data shows that the calculated transition energy values are larger than the experimentally measured and that the differences in transition energy increase with increasing energy (i.e., the larger the transition energy the larger the error). The root-mean square deviation of the results at this level ($\lambda^{Os}=1.00$) is 2360 cm^{-1}. Previous studies in our laboratory[35] have shown that these discrepancies are due to approximations in the treatment of both spin-orbit coupling and electron correlation, and that these discrepancies should show also in the cluster calculations. We will analyze them and try to find corrections to them that can be transferred to solid state calculations of the embedded ion. First of all we can see that the calculated spin-orbit splittings of the spin-free terms are larger than the splittings experimentally determined. This suggests that the Os contribution to the spin-orbit operator should be reduced. Following Refs. 35 and 36, we have reduced the scaling factor λ^{Os} from its starting value of 1.00 to the value of 0.90. The results of the spin-orbit calculations using this $\lambda^{Os}=0.90$ value are shown in the third column of Table I and in the (b) part of Fig. 1. We can see that the deviations with respect to the experiment decrease notably by using this factor, with the root-mean square deviation being 707 cm^{-1}.

The results of this calculation show that significant discrepancies remain for some of the spin-orbit states. These discrepancies can now be attributed to incomplete treatment of dynamical electron correlation. From Table I, we can see that the errors are of the order of -400 cm^{-1} for the spin-orbit components of the $1\,^3P$, of the order of 300–800 cm^{-1} for most of the components of the $1\,^3F$, ^3D, ^3H, and ^3G states, and around 1100–1400 cm^{-1} for the ^1F, ^1I, $1\,^1D$, and $1\,^1G$ states. Then, we performed a new sfss calculation modifying the δ parameters, Eq. (2), for the states we have just mentioned. We added corrections of 400 cm^{-1} to $\delta(1\,^3P)$; -500 cm^{-1} to $\delta(1\,^3F)$, $\delta(^3D)$, $\delta(^3H)$, and $\delta(^3G)$; -1200 cm^{-1} to $\delta(^1F)$, $\delta(^1I)$, $\delta(1\,^1D)$, and $\delta(1\,^1G)$. The results of this calculation are shown in Table I, under the heading "$\lambda^{Os}=0.90$ (corrected)." The final root-mean square deviation with respect to the experiment is 410 cm^{-1}. We will transport the corrections found in this section to the study of the spectroscopy of the Os^{4+} ion as a dopant in halide lattices, presented below.

Together with the transition energies, we present the composition of the spin-orbit states in terms of spin-free states for this calculation. We present those terms that have at least 15% weight in the spin-orbit wave function. This composition is similar to the composition found in the calculations with $\lambda^{Os}=1.00$ and $\lambda^{Os}=0.90$, the differences being lower than 5%. A similar decomposition can be found in Ref. 54, based in semiempirical calculations. Unfortunately, the spin-free levels in Ref. 54 are classified according to a seniority number criterion. The spin-free levels that belong to the same S and L are rotated between them in order to find a diagonal representation of another operator, sometimes denoted as Q.[55] Then, our calculated weights for spin-free levels that appear more than once in the d^4 configuration (^3P, ^3F, ^1S, ^1D, and ^1G) are not directly comparable to the ones quoted in Ref. 54. We include in the last column of the table the weight of the leading spin-free level taken from Ref. 54. For the comparable terms, the agreement of our calculated weights is good.

IV. STRUCTURE AND SPECTROSCOPY OF Os^{4+}-DOPED Cs_2GeF_6 AND Cs_2ZrCl_6

A. Local structure of $(OsF_6)^{2-}$ and $(OsCl_6)^{2-}$ embedded clusters

We have optimized the local structure of the cluster both for $(OsF_6)^{2-}$ and $(OsCl_6)^{2-}$ in all the states coming from the t_{2g}^4 and $t_{2g}^3e_g^1$ electron configurations. We have calculated the equilibrium Os–X distance R_e, the breathing mode (a_{1g} symmetric) vibrational frequency of the cluster $\bar{\nu}_{a_{1g}}$, and the minimum-to-minimum transition energy relative to the ground state, T_e; the results of the calculations are presented in Table II and Fig. 2 for the fluoride compound and in Table III and Fig. 3 for the chloride. In the tables, together with the results, we present the spin-free parentage of the spin-orbit levels and the free ion term to which these spin-free "parent" states are correlated. It should be noticed that, although it is costumarily done, the assigment of the spin-orbit to spin-free states is only approximate. We have also shown in the tables the dominant spatial electron configuration of the different states.

We start by commenting the results for the fluoride cluster. From Table II and Fig. 2, we see that our calculations

TABLE I. Results for the *d-d* spectrum of Os^{+4}, as calculated in this work and experimental measurements from Ref. 54. Numbers are in cm^{-1}. In parentheses, composition of the spin-orbit levels in terms of spin-levels. States marked with an asterisk are not included in the δ correction procedure.

	sfss spin-orbit calculations					
State	$\lambda^{Os}=1.0$	$\lambda^{Os}=0.90$	$\lambda^{Os}=0.90$	(corrected)	Experiment[a]	
$J=0$						
	0	0	0	(68.08 ^5D 28.19 1 ^3P)	0	(64 ^5D)
	19 214	17 900	17 870	(54.72 1 ^3P 30.65 ^5D)	18 364	(35 ^5D)
	46 493	43 919	42 957	(77.84 1 ^1S 16.95 1 ^3P)		
	*65 086	62 254	62 101	(91.09 2 ^3P)		
$J=1$						
	4607	3788	3755	(86.09 ^5D)	4311	(84 ^5D)
	25 976	24 239	24 426	(79.35 1 ^3P)	24 680	(53 $_4$ ^3P)
	41 103	38 709	38 203	(89.01 ^3D)	38 536	(86 ^3D)
	*61 513	59 942	58 851	(98.19 2 ^3P)	55 988	(61 $_2$ ^3P)
$J=2$						
	8650	7327	7232	(92.82 ^5D)	8083	(91 ^5D)
	26 373	25 100	24 449	(73.10 1 ^3F 15.65 1 ^1D)	24 401	(48 $_4$ ^3F)
	32 202	30 343	30 260	(52.34 1 ^3P 39.18 ^3D)	30 247	(43 $_4$ ^3P)
	39 061	36 853	36 346	(30.42 1 ^1D 25.19 1 ^3P 22.02 ^3D 15.65 1 ^3F)	36 307	(22 $_4$ ^1D)
	47 453	45 077	44 560	(33.23 1 ^1D 22.49 ^3D 16.57 1 ^3P 15.82 2 ^3F)	43 960	(33 $_4$ ^3P)
	54 781	52 821	52 679	(75.09 2 ^3P 15.64 2 ^3F)	49 999	(57 $_2$ ^3P)
	*59 292	56 500	56 204	(64.62 2 ^3F 15.26 1 ^1D)	55 043	(36 $_2$ ^3F)
$J=3$						
	11 778	10 222	10 084	(89.07 ^5D)	11 018	(87 ^5D)
	25 970	24 672	24 100	(58.71 ^3G 29.27 1 ^3F)	23 942	(62 ^3G)
	34 638	32 836	32 207	(51.02 1 ^3F 21.91 ^3D)	32 171	(51 $_4$ ^3F)
	37 191	34 989	34 421	(54.76 ^3D 22.53 ^3G)	34 704	(41 ^3D)
	50 241	47 842	46 820	(69.01 ^1F 17.09 ^3D)	46 548	(63 ^1F)
	*59 920	57 304	57 018	(83.23 2 ^3F)	55 872	(64 $_2$ ^3F)
$J=4$						
	13 938	12 440	12 216	(73.82 ^5D 19.76 1 ^3F)	12 966	(67 ^5D)
	22 332	21 141	20 537	(56.59 ^3H)	20 374	(57 ^3H)
	32 314	30 259	29 688	(42.68 ^3G 24.43 ^3H 21.88 1 ^3F)	29 844	(55 ^3G)
	34 160	32 039	31 336	(29.93 1 ^3F 29.90 1 ^1G 26.20 ^3G)	31 788	(39 $_4$ ^3F)
	47 042	44 344	43 505	(47.25 1 ^1G 17.59 1 ^3F)	43 779	(43 $_4$ ^1G)
	57 661	55 031	54 822	(70.61 2 ^3F)	53 795	(65 $_2$ ^3F)
	*64 935	62 446	62 345	(83.35 2 ^1G)	59 575	(50 $_2$ ^1G)
$J=5$						
	27 804	26 165	25 579	(77.18 ^3H 22.73 ^3G)	25 343	(76 ^3H)
	40 064	37 368	36 781	(77.18 ^3G 22.74 ^3H)	37 015	(76 ^3G)
$J=6$						
	30 515	28 727	27 990	(77.39 ^3H 22.53 ^1I)	27 669	(74 ^3H)
	43 232	40 681	39 545	(77.39 ^1I 22.54 ^3H)	39 283	(74 ^1I)
rms[b]						
	2360	707	410			

[a]The subscript number preceeding certain terms is the seniority number.
[b]Root-mean square deviation relative to experimental data, including all spin-orbit states below 50 000 cm^{-1}.

predict two different manifolds of states, with different properties between them and composed of states that share very similar spectroscopic constants. All the states belonging to the t_{2g}^4 configuration, including the $1\,A_{1g}$ ground state, have an equilibrium distance of the order of 1.941 Å (±0.003 Å) and a $\bar{\nu}_{a_{1g}}$ vibrational frequency of around 628 cm^{-1} (±3 cm^{-1}). All the states coming from the $t_{2g}^3 e_g^1$ configuration form an almost parallel set, with a larger equilibrium distance than the states belonging to the t_{2g}^4 configuration, around 1.988 Å. The breathing vibrational frequency for these states is smaller, by some 15–25 cm^{-1}, than that corresponding to the first set, except for some of the highest lying excited states, which present somewhat different values due to mixing with $t_{2g}^2 e_g^2$ states. This is a typical situation for transition-metal impurities, the equilibrium distance correlates very well with the different orbital occupancy: the

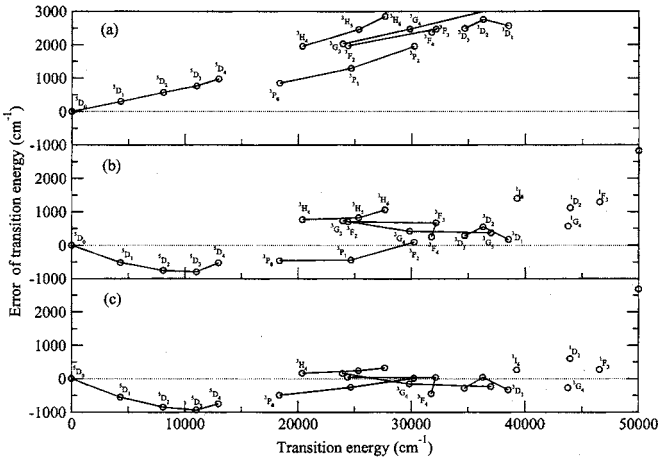

FIG. 1. Errors of the calculated Os^{4+} free ion transition energies with respect to experimental values, taken from Ref. 54. (a) $\lambda^{Os}=1.00$ results. (b) $\lambda^{Os}=0.90$ results, including ^1L_J states. (c) $\lambda^{Os}=0.90$ (corrected) results, including ^1L_J states.

larger the occupancy of the (antibonding) e_g orbitals, the larger the equilibrium distance. This fact shows that even in the case of 5*d* transition-metal ions, in which the spin-orbit coupling is very important, the spin-free strong field labels seem to be valid. The distortion from the undoped Cs_2GeF_6 lattice induced by the impurity is a relatively large outward distortion, as the Ge–F in the perfect lattice is 1.804 Å.[22] That displacement is larger than the mismatch of ionic radii of Os^{4+} and Ge^{4+}, which amounts to some 0.09 Å.[56]

To our knowledge, there are not experimental determinations of the equilibrium distance or the vibrational frequency $\bar{\nu}_{a_{1g}}$ for the ground state of $Os^{4+}:Cs_2GeF_6$. From 15 K emission spectra,[7] values for this frequency are derived for excited states, around 560 cm^{-1} for the $1\,T_{1g}$ state and around 590 cm^{-1} for the $1\,T_{2g}$ state. We calculate these numbers to be very similar to the ones for the ground state, so we think that these experimental results do not really correspond to the a_{1g} vibrational frequency. In fact, in Ref. 7, the authors point that the experimental luminescence spectrum is plenty of overlapping lines that cannot be assigned unambiguously (especially, the emission to the $1\,T_{1g}$ state). Due to this fact, only tentative explanations for most of the lines are given. It should be noticed too that, due to the very small difference in equilibrium distance between all the states monitored in Ref. 7, progressions in the a_{1g} are very short, so that usually only the second term of a progression is seen and this one with a very small intensity, making the assignments more difficult. Values of the $\bar{\nu}_{a_{1g}}$ vibrational frequency are available in the literature for pure Cs_2GeF_6 (610 cm^{-1}) (Ref. 57) and Cs_2OsF_6 (608 cm^{-1}),[58] and we expect this frequency to be very similar in the doped compound. Assuming a value of 609 cm^{-1} our calculated values for $(OsF_6)^{2-}$ deviate some 3% from these values.

The results for the chloride cluster (Table III and Fig. 3) are quite similar to the ones for the fluoride. Two manifolds of nearly parallel states are found, corresponding to the t_{2g}^4 and $t_{2g}^3e_g^1$ electron configurations. The equilibrium distance for the $t_{2g}^3e_g^1$ states is appreciably larger than that of the t_{2g}^4 states, and the a_{1g} vibrational frequency is lower by some 10–15 cm^{-1}. The Zr–Cl distance in the host Cs_2ZrCl_6 lattice is 2.446 Å,[22] so the distortion with respect to the perfect Cs_2ZrCl_6 lattice is a compression in this case, consistent with the mismatch of ionic radii between Os^{4+} and Zr^{4+}, around −0.09 Å.[56] Again the only comparable experimental data refer to the breathing mode vibrational frequency $\bar{\nu}_{a_{1g}}$. From Raman spectra,[10] this frequency is 340 cm^{-1} for the ground state, and from luminescence spectroscopy, the same authors[10] found a value of 338 cm^{-1} for $Os^{4+}:Cs_2ZrCl_6$. Our result of 355 cm^{-1} is larger by around 15 cm^{-1} (around 4.5%) in line with the discrepancies found in previous works for similar systems.[29] In different chloride lattices or in solution, values in the range of 340–360 cm^{-1} are found.[10,14,16–20,59] From absorption[9,11] and luminescence spectra[10] in $Os^{4+}:Cs_2ZrCl_6$, values around 340 cm^{-1} are also found for this vibrational frequency in excited states coming from the same electron configuration as the ground state (t_{2g}^4), also in line with our calculations, which predict all these states to be almost parallel. The only exception is the $2\,T_{2g}$ state, whose frequency is estimated to be quite high [380 cm^{-1} (Ref. 9) and 400 cm^{-1} (Ref. 11)], in disagreement with the fact that, due to the intraconfigurational character of the transition to this state, the $\bar{\nu}_{a_{1g}}$ frequency is expected to be similar to the one of the ground state. We will return later to this point, when discussing the electronic transition energies. Again, in similar doped systems,[15–17] the vibrational frequency found for these intraconfigurational excited states is in the range of 335–350 cm^{-1}.

B. Electronic transitions of $Cs_2GeF_6:(OsF_6)^{2-}$ and $Cs_2ZrCl_6:(OsCl_6)^{2-}$

Together with the structural results, in Tables II and III, we can find the minimum-to-minimum transition energies between the ground state and the different excited states. As the vibrational frequencies are similar in the states studied here, these energies should be comparable to the experimental zero-phonon transition energies. We will first make a comparison between the results found for both hosts and then make a more detailed comparison with the experimental spectra.

We can see that, for both hosts, the structure of the spectrum is quite similar: the lowest lying states are those coming from the spin-free $^3T_{1g}$ state, split by spin-orbit interaction by some 6400 cm^{-1} (fluoride host) or 5600 cm^{-1} (chloride host). The different states related to spin-free singlet states of the t_{2g}^4 configuration are found next. Due to the quite large ligand field, all the states from the $t_{2g}^3e_g^1$ electron configuration lie higher in energy. The first group of states, related to the spin-free ^5E_g state [we will refer to them collectively as (^5E_g) levels], is higher than the $2\,A_{1g}(^1A_{1g})$ state by around 1500 cm^{-1} in the fluoride and 3300 cm^{-1} in the chloride. Above that, we find the rest of the $t_{2g}^3e_g^1$ manifold of states, covering a large region of some 31 000 cm^{-1} in the fluoride and 23 000 cm^{-1} in the chloride. The ordering of the states within this manifold is similar for both hosts. All the transitions are higher in energy in the fluoride than in the chloride, due to the higher ligand field promoted by the F^- ions.

TABLE II. Spectroscopic constants of the $(OsF_6)^{2-}$ cluster. Distances are in Å, and frequencies and energies are in cm^{-1}.

State	Spin-free parentage[a]	R_e	$\bar{\nu}_{a1_g}$	T_e	Ref. 7
	t_{2g}^4 configuration				
$1\,A_{1g}$	84.65 $^3T_{1g}(^3H)$	1.943	626	0	0
$1\,T_{1g}$	94.08 $^3T_{1g}(^3H)$	1.941	630	3753	3255[b]
$1\,T_{2g}$	77.41 $^3T_{1g}(^3H)$	1.940	631	6124	5956[b]
$1\,E_g$	83.44 $^3T_{1g}(^3H)$	1.940	630	6370	6000[b]
$2\,T_{2g}$	76.09 $^1T_{2g}(^1I)$	1.940	629	13 326	12 693[b]
$2\,E_g$	83.51 $^1E_g(^1I)$	1.939	631	14 168	12 936[b]
$2\,A_{1g}$	84.42 $^1A_{1g}(^1I)$	1.944	625	22 566	21 790[b]
	$t_{2g}^3e_g^1$ configuration				
$1\,A_{2g}$	95.48 $^5E_g(^5D)$	1.989	606	24 043	23 000–30 000[c]
$3\,T_{2g}$	93.02 $^5E_g(^5D)$	1.989	608	24 122	
$3\,E_g$	90.97 $^5E_g(^5D)$	1.988	610	24 234	
$2\,T_{1g}$	88.24 $^5E_g(^5D)$	1.988	610	24 296	
$3\,A_{1g}$	85.53 $^5E_g(^5D)$	1.989	604	24 449	
$3\,T_{1g}$	40.31 $^3E_g(^3H)$	1.990	601	31 828	30 000–40 000[d]
$4\,A_{1g}$	86.08 $^3T_{1g}(^3H)$	1.987	611	33 441	
$4\,T_{1g}$	43.97 $^3T_{1g}(^3H)$	1.989	604	33 799	
$4\,T_{2g}$	82.19 $^3E_g(^3H)$	1.990	600	33 958	
$4\,E_g$	77.70 $^3T_{2g}(^3H)$	1.988	607	34 565	
$5\,T_{1g}$	56.25 $^3T_{2g}(^3H)$	1.990	603	35 283	
$5\,T_{2g}$	56.81 $^3T_{2g}(^3H)$	1.989	604	35 759	
$6\,T_{2g}$	33.16 $^3A_{2g}(1\,^3F)$	1.990	601	36 074	
$6\,T_{1g}$	81.94 $^3A_{1g}(^3G)$	1.989	603	36 730	
$5\,E_g$	87.80 $^3T_{1g}(^3H)$	1.987	607	36 936	
$7\,T_{2g}$	42.77 $^3T_{1g}(^3H)$	1.988	606	37 065	
$2\,A_{2g}$	78.16 $^3T_{2g}(^3H)$	1.988	604	37 741	
$7\,T_{1g}$	92.78 $^3E_g(^3G)$	1.989	602	38 405	
$8\,T_{2g}$	52.71 $^3E_g(^3G)$	1.988	605	38 507	
$3\,A_{2g}$	69.89 $^1A_{2g}(^1I)$	1.987	606	40 376	
$9\,T_{2g}$	67.47 $^1T_{2g}(^1I)$	1.989	602	40 380	
$6\,E_g$	82.33 $^1E_g(^1G)$	1.989	602	41 476	
$8\,T_{1g}$	81.01 $^1T_{1g}(^1I)$	1.989	602	41 990	
$4\,A_{2g}$	78.51 $^3T_{2g}(1\,^3F)$	1.988	603	46 126	
$5\,A_{1g}$	73.65 $^1A_{1g}(1\,^1G)$	1.986	603	46 699	
$10\,T_{2g}$	52.57 $^3T_{2g}(1\,^3P)$	1.989	589	47 441	
$7\,E_g$	75.59 $^3T_{1g}(1\,^3P)$	1.989	595	47 716	
$11\,T_{2g}$	62.31 $^3T_{2g}(1\,^3F)$	1.989	604	47 747	
$9\,T_{1g}$	67.11 $^3T_{1g}(1\,^3P)$	1.992	583	48 291	
$10\,T_{1g}$	86.94 $^3T_{2g}(1\,^3F)$	1.988	601	49 320	
$8\,E_g$	71.64 $^3T_{2g}(1\,^3F)$	1.988	601	50 115	
$6\,A_{1g}$	65.22 $^3T_{1g}(1\,^3P)$	1.994	567	50 711	
$11\,T_{1g}$	77.09 $^1T_{1g}(1\,^1G)$	1.987	618	52 988	
$12\,T_{2g}$	87.74 $^1T_{2g}(1\,^1G)$	1.990	590	54 704	

[a]Largest weight of a spin-free wave function in the state, given in % and calculated at $R(\text{Os–F})=3.65$ a.u. $=1.932$ Å.
[b]Estimated from the observed vibronic peaks.
[c]Weak and broad absorptions.
[d]Moderately intense and broad absorptions.

We will make now a comparison of our calculated results with the experimental results. $Os^{4+}:Cs_2GeF_6$ has received little attention in the past, in contrast to its chloride analog. Absorption and magnetic circular dichroism (MCD) spectra for energies higher than 25 500 cm^{-1} were reported,[21] and the strong bands found there were assigned to *d-d* transitions of the $(OsF_6)^{2-}$ chromophore. This assignment has been strongly criticized especially in Ref. 7 on intensity grounds. The deviations between our calculated transitions and the corresponding transitions in the experiment are very large, of around 7000–8000 cm^{-1}. This fact reinforces the conclusion of a different origin for these bands. Beside that, only diffuse reflectance spectra of K_2OsF_6 (Ref. 13) were reported. More recently, detailed absorption and luminescence spectra of Os^{4+}-doped Cs_2GeF_6 have been reported.[7]

The absorption spectrum of Ref. 7 is composed, below 23 000 cm^{-1}, by three groups of sharp lines: the most intense, located around 6500 cm^{-1}, is assigned to transitions to

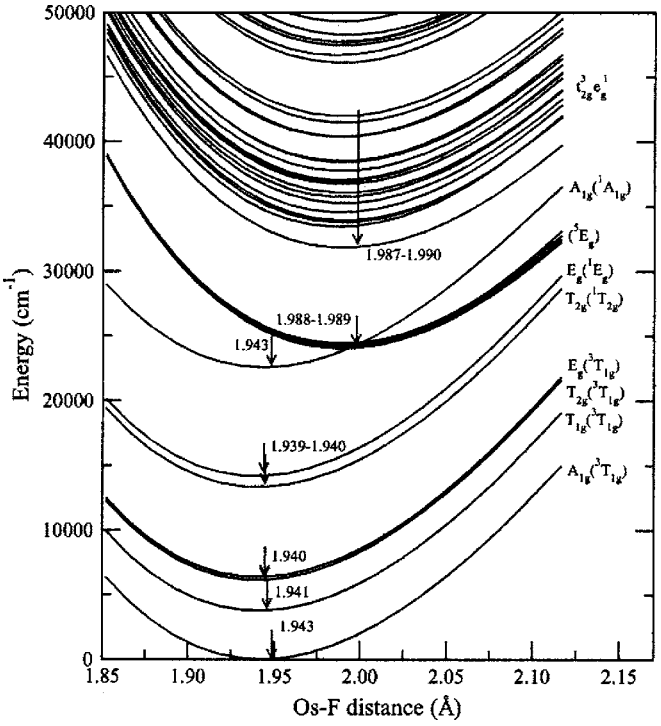

FIG. 2. Potential energy curves of the ground and lowest excited states of the $(OsF_6)^{2-}$ cluster as a function of the Os–F distance in the a_{1g} vibrational mode. The results correspond to spin-orbit ssfs-CASPT2 WB-AIMP calculations.

the 1 T_{2g}/1 E_g levels and two weaker groups, located around 13 500 and 22 000 cm^{-1}, are assigned to transitions to the 2 T_{2g}/2 E_g and 2 A_{1g} levels, respectively. Weak absorptions are observed between 23 000 and 30 000 cm^{-1}, followed by moderately intense broad absorption bands above 30 000 cm^{-1}.[7] All the electronic transitions below 23 000 cm^{-1} are strongly forbidden in the solid, and no 0-0 line is seen neither in absorption nor in luminescence experiments. Their position is then estimated from analysis of the vibrational structure of the spectrum. The values for these lines, estimated in this way in Ref. 7, are shown in Table II. The weak and broad bands between 23 000 and 30 000 cm^{-1} are assigned to the spin-allowed interconfigurational *d-d* transitions of $(OsF_6)^{2-}$, while the origin of the moderately intense bands above 30 000 cm^{-1} is not clear and no assignment is made in Ref. 7. This assignment implies that the (^5E_g) spin-orbit levels should lie around 16 000 cm^{-1}, immersed and unobserved, in the t_{2g}^4 manifold energy range.

Our calculations provide data that suggest a reinterpretation of the experimental facts. In the region below 23 000 cm^{-1} our assigment is the same with that of Ref. 7. The agreement of our calculated transitions with the estimated zero-phonon lines is good in general, with differences of some 5%, except for the transition to the 2 E_g state which presents a deviation of around 10%. We will comment on this point later on. On the other hand, above 23 000 cm^{-1} our calculations suggest a different assignment: the weak absorptions between 23 000 and 30 000 cm^{-1} can be attributed to transitions to the different spin-orbit levels related to the ^5E_g spin-free state. The relatively more intense absorption bands located between 30 000 and 40 000 cm^{-1} can be interpreted as multiple origins of spin-allowed absorption bands, predominantly of triplet-triplet character, associated with transitions to the 3 T_{1g}–8 T_{2g} states. Due to the different equilibrium distance of the states implicated, these transitions are expected to be seen as broad bands, consistently with the experimental facts.

In conclusion, our results allow to describe and are consistent with all the different spectral features of the absorption spectrum: the weak and sharp groups of lines, the weak and broad, and the moderately intense and broad bands. Our results clearly describe the *d-d* spectrum as formed by two

TABLE III. Spectroscopic constants of the $(OsCl_6)^{2-}$ cluster. Distances are in Å, and frequencies and energies are in cm^{-1}.

State	Spin-free parentage[a]	R_e	$\bar{\nu}_{a1_g}$	T_e
	t_{2g}^4 configuration			
1 A_{1g}	84.46 $^3T_{1g}(^3H)$	2.338	355	0
1 T_{1g}	94.81 $^3T_{1g}(^3H)$	2.335	358	3366
1 T_{2g}	75.27 $^3T_{1g}(^3H)$	2.333	359	5317
1 E_g	83.22 $^3T_{1g}(^3H)$	2.333	359	5625
2 T_{2g}	74.13 $^1T_{2g}(^1I)$	2.331	359	11 348
2 E_g	82.94 $^1E_g(^1I)$	2.330	359	12 333
2 A_{1g}	83.85 $^1A_{1g}(^1I)$	2.334	345	18 753
	$t_{2g}^3e_g^1$ configuration			
1 A_{2g}	93.77 $^5E_g(^5D)$	2.390	339	22 066
3 T_{2g}	91.08 $^5E_g(^5D)$	2.389	340	22 077
2 T_{1g}	85.22 $^5E_g(^5D)$	2.389	340	22 109
3 E_g	88.82 $^5E_g(^5D)$	2.389	341	22 117
3 A_{1g}	83.32 $^5E_g(^5D)$	2.387	343	22 233
3 T_{1g}	48.36 $^3E_g(^3H)$	2.386	338	26 908
4 T_{2g}	78.61 $^3E_g(^3H)$	2.385	339	28 493
4 A_{1g}	84.41 $^3T_{1g}(^3H)$	2.383	341	28 915
4 T_{1g}	46.35 $^3T_{1g}(^3H)$	2.384	340	29 203
4 E_g	74.71 $^3T_{2g}(^3H)$	2.384	340	29 693
5 T_{1g}	59.55 $^3T_{2g}(^3H)$	2.385	339	30 253
5 T_{2g}	47.55 $^3T_{2g}(^3H)$	2.383	340	30 536
6 T_{2g}	35.11 $^3T_{1g}(^3H)$	2.384	339	31 253
5 E_g	85.97 $^3T_{1g}(^3H)$	2.382	341	31 815
6 T_{1g}	80.66 $^3A_{1g}(^3G)$	2.382	341	31 900
7 T_{2g}	47.93 $^3A_{2g}(1\ ^3F)$	2.383	340	31 980
2 A_{2g}	58.72 $^3T_{2g}(^3H)$	2.383	339	32 171
7 T_{1g}	87.92 $^3E_g(^3G)$	2.382	339	32 719
8 T_{2g}	46.47 $^3E_g(^3G)$	2.382	340	32 938
3 A_{2g}	49.64 $^1A_{2g}(^1I)$	2.381	340	33 630
9 T_{2g}	60.71 $^1T_{2g}(^1I)$	2.383	339	33 822
6 E_g	80.18 $^1E_g(1\ ^1G)$	2.382	338	34 422
8 T_{1g}	75.59 $^1T_{1g}(^1I)$	2.381	339	34 867
5 A_{1g}	85.71 $^1A_{1g}(1\ ^1G)$	2.376	337	38 030
4 A_{2g}	72.99 $^3T_{2g}(1\ ^3F)$	2.381	338	39 110
10 T_{2g}	64.48 $^3T_{1g}(1\ ^3P)$	2.382	333	40 042
7 E_g	74.11 $^3T_{1g}(1\ ^3P)$	2.382	334	40 149
11 T_{2g}	45.71 $^3T_{2g}(1\ ^3F)$	2.380	339	40 429
9 T_{1g}	53.55 $^3T_{1g}(1\ ^3P)$	2.383	332	40 555
10 T_{1g}	83.03 $^3T_{2g}(1\ ^3F)$	2.381	337	41 695
8 E_g	69.66 $^3T_{2g}(1\ ^3F)$	2.380	338	42 376
6 A_{1g}	76.81 $^3T_{1g}(1\ ^3P)$	2.385	325	42 763
11 T_{1g}	62.75 $^1T_{1g}(1\ ^1G)$	2.382	333	43 980
12 T_{2g}	84.71 $^1T_{2g}(1\ ^1G)$	2.380	334	45 138

[a]Largest weight of a spin-free wave function in the state, given in % and calculated at R(Os–Cl)=4.40 a.u.=2.328 Å.

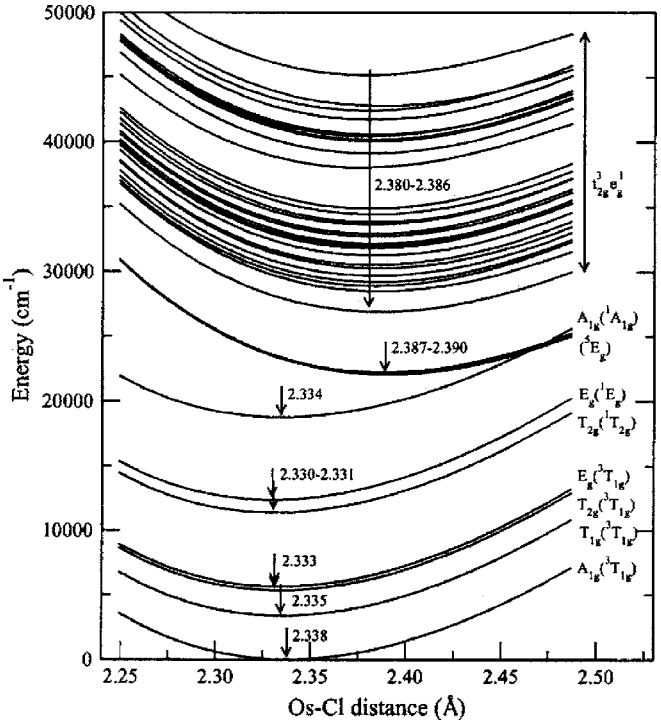

FIG. 3. Potential energy curves of the ground and lowest excited states of the $(OsCl_6)^{2-}$ cluster as a function of the Os–Cl distance in the a_{1g} vibrational mode. The results correspond to spin-orbit ssfs-CASPT2 WB-AIMP calculations.

subsequent manifolds associated with t_{2g}^4 and $t_{2g}^3e_g^1$ electron configurations and separated by an energy gap of around 1500 cm^{-1}.

We focus now on the chloride cluster results. As we pointed out before, this chromophore was more widely studied in the past than the fluoride analog. As a result, absorption,[2,7–9,11] luminescence,[2,10] and MCD[9,11] spectra were presented for Os^{4+}-doped Cs_2ZrCl_6, and the $(OsCl_6)^{2-}$ chromophore has also been studied in some other crystals[12,15,16,18] and in solution.[20] Most of them focused on the lower energy part of the spectrum, where several groups of sharp lines are found, in close resemblance to the fluoride cluster spectrum. These features are assigned to transitions between the different spin-orbit levels related to the t_{2g}^4 electron configuration. We present in Table IV the values of the zero-phonon energies for these transitions, as estimated from the analysis of vibronic peaks of the different bands in the experimental works, together with our calculated results for the same transitions, in order to facilitate the comparison between them.

By looking at Table IV, we see that our calculated spectrum provides the same assignments as the experiments. The deviations from the estimated experimental energies are of the order of 10%, in line with the results for the fluoride cluster. However, for the $2\,E_g$ state we found a difference of some 1400 cm^{-1} with respect to the absorption spectrum of Ref. 11, a discrepancy somewhat larger than expected. It is worth pointing out that some controversy exists in the experimental side for this $1\,A_{1g}\rightarrow 2\,E_g$ transition. Kozikowski and Kiederling[11] give a value of 10 918 cm^{-1} for the 0-0 line of this transition from the vibrational analysis of the absorption spectrum of $Os^{4+}:Cs_2ZrCl_6$. Wermuth and Güdel,[2] more recently, give the similar value of 10 925 cm^{-1} without offering great details about the assignments, but Flint and Paulusz[16] give a result of 11 952 cm^{-1} for the same transition in Os^{4+}-doped Cs_2TeCl_6 based in their analysis of emission spectra. The difference between both numbers is quite large, around 1000 cm^{-1}. An intermediate value of 11 102 cm^{-1} has been given[8] from the older spectrum of $Os^{4+}:K_2PtCl_6$. In the same host, a value of 10 939 cm^{-1} is quoted in Ref. 18, but no more details are found there. Although the results of Ref. 16 correspond to a different chloride lattice (Cs_2TeCl_6), the rest of the transitions are very close to the Cs_2ZrCl_6 results and we should expect this transition to be close too. This transition occurs, in absorption, in a region where the intensity of absorption related to the $2\,T_{2g}$ state is still important, making the assignment of the lines difficult. In this line, all the absorptions in this region are assigned to $1\,A_{1g}\rightarrow 2\,T_{2g}$ vibronic bands, which is according to Ref. 9. The assignment of Flint and Paulusz[16] has been criticized, first by themselves in the same paper, as it is difficult to explain why luminescence can be seen from the $2\,E_g$ state, lying only 1400 cm^{-1} above the $2\,T_{2g}$ state (less than five a_{1g} vibrational quanta); and later by Kozikowski and Kiederling,[18] which gives another assignment for the same lines. In the case that the assignment of Ref. 16 was wrong, there are a number of features in absorption spectra that remain unassigned in this spectral region. As pointed out by Flint and Paulusz,[16] spectral features up to some 1700 cm^{-1} from the origin of the $1\,A_{1g}\rightarrow 2\,T_{2g}$ transition have been detected and they are either unassigned[9] or assigned to an a_{1g} progression

TABLE IV. Theoretical and experimental transition energies, estimated from vibronic origin analysis, for the t_{2g}^4 intraconfigurational spectrum of embedded $(OsCl_6)^{2-}$. Energies are in cm^{-1}.

			$Os^{4+}:Cs_2ZrCl_6$				$Os^{4+}:Cs_2TeCl_6$	$Os^{4+}:K_2PtCl_6$	
	State	This work	Ref. 9	Ref. 10	Ref. 11	Ref. 2	Ref. 16	Ref. 8	Ref. 18
$1\,A_{1g}$	84.46 $^3T_{1g}(^3H)$	0	0	0	0	0	0	0	0
$1\,T_{1g}$	94.81 $^3T_{1g}(^3H)$	3366		2777	2779	2778	2786		
$1\,T_{2g}$	75.27 $^3T_{1g}(^3H)$	5317	4870	4873	4876	4870	4884		4908
$1\,E_g$	83.22 $^3T_{1g}(^3H)$	5625		4972	4975	4970	4983		5008
$2\,T_{2g}$	74.13 $^1T_{2g}(^1I)$	11 348	10 510		10 514	10 515	10 520	10 561	10 555
$2\,E_g$	82.94 $^1E_g(^1I)$	12 333			10 918	10 925	11 952	11 102	10 939
$2\,A_{1g}$	83.85 $^1A_{1g}(^1I)$	18 753	17 061	17 069	17 068	17 066	17 025	17 090	17 099

based on the $1A_{1g} \rightarrow 2T_{2g}$ transition[11] by using an a_{1g} vibrational frequency quite large (around 400 cm^{-1}, in contrast to the value of around 350 cm^{-1} found for other transitions). According to Flint and Paulusz,[16] a separation of at least 1000 cm^{-1} between the origins of both transitions can explain most of the experimental findings. Our results show a separation of around 1000 cm^{-1}, giving support to the suggestions of Ref. 16.

The same line of reasoning can be used in the case of the fluoride cluster. There, the difference between the origins of the corresponding transitions is estimated to be 243 cm^{-1},[7] while we predict some 850 cm^{-1} (see Table II). Again, features up to 2100 cm^{-1} from the origin of the $1A_{1g} \rightarrow 2T_{2g}$ transition are reported in absorption, a significant number of them unassigned. We think that it is not unreasonable to locate the second electronic origin ($1A_{1g} \rightarrow 2E_g$ transition) at a larger energy, as suggested by our calculations.

In the chloride compound, the more energetic intraconfigurational transition ($1A_{1g} \rightarrow 2A_{1g}$) is calculated by us with an error of around 1700 cm^{-1}. This error is larger (more than twice) than the error found in the fluoride. Part of this larger error may be due to the fact that ligand-to-metal charge transfer (CT) configurations are not included in the zeroth-order wave functions for the correlation treatment. These configurations are located at much smaller energies in the chloride than in the fluoride compound, and can have more importance in the former than in the latter.

Turning now to the interconfigurational transitions, it should be pointed out that no experimental determination of these energies exists as the transition in the corresponding spectral region (more than 20 000 cm^{-1}) is dominated by CT bands, some of them allowed and then very intense. In Ref. 8, a number of bands in this region were assigned to these *d-d* transitions, but later it was firmly established that they were CT bands.[9] Then, no comparison to experimental energies can be made. The lowest lying of this manifold of transitions is the $1A_{1g} \rightarrow ({}^5E_g)$ transition, which our results predict to be around 22 000 cm^{-1}, split by some 170 cm^{-1}. The gap between these states and the top of the t_{2g}^4 manifold is about 3300 cm^{-1}. No definite determination of the transition energy to the $({}^5E_g)$ states has been provided, although values ranging from 16 000 to 21000 cm^{-1} have been suggested in the literature from estimations.[9,11,13,18] In a specific search for this state, Kozikowsky and Kiederling[18] did not find any hint of it lying lower than 20 400 cm^{-1}. In this point we would like to pay some attention to a broad band, centered around 22 000 cm^{-1}, reported from absorption spectra.[2] A similar band can be seen in the spectrum of $(OsCl_6)^{2-}$ in solution in Ref. 20. (Note that no band in this energy region is reported in Ref. 9). This band has been claimed not to belong to the spectrum of the main Os^{4+} species,[2] because the fine structure of its luminescence is different from that of the main species. In spite of that, our calculations suggests that this transition can be the $1A_{1g} \rightarrow ({}^5E_g)$ transition. It should be broad, due to the difference in equilibrium distance between the states involved. The experimental band intensity is quite large, in spite of it being strongly forbidden. However, according to our results, the percentage of spin triplet states in these spin-orbit states is of the order of 15%, relaxing somewhat the spin prohibition. The close presence of CT bands may enhance the intensity of this transition too. Although its large intensity remains to be fully explained, we think that it is reasonable to assign this band to the $1A_{1g} \rightarrow ({}^5E_g)$ transition.

TABLE V. Theoretical and experimental decrease of the transition energies for the intraconfigurational spectrum of Os^{4+} in both fluoride and chloride hosts, in cm^{-1}.

Transition		This work	Experiment[a]
$1A_{1g}$	${}^3T_{1g}({}^3H)$	0	0
$1T_{1g}$	${}^3T_{1g}({}^3H)$	387	476
$1T_{2g}$	${}^3T_{1g}({}^3H)$	807	1080
$1E_g$	${}^3T_{1g}({}^3H)$	745	1025
$2T_{2g}$	${}^1T_{2g}({}^1I)$	1978	2179
$2E_g$	${}^1E_g({}^1I)$	1835	2018
$2A_{1g}$	${}^1A_{1g}({}^1I)$	3813	4722

[a]References 7 and 11.

V. EFFECTS OF LIGAND SUBSTITUTION ON THE LUMINESCENCE OF Os^{4+}

From the previous sections, we have a reliable estimation of the position of the different excited states of the clusters and of totally symmetric vibrational frequencies $\bar{\nu}_{a_{1g}}$. From a combined look at Tables II and III, we can see the effect on the electronic transitions of the Os^{4+} ions due to the change in the ligand, which can be seen also in Table V. There, we present the decrease of the transition energy in going from the fluoride to the chloride cluster, for the intraconfigurational spectrum, as calculated by us and experimentally determined (we use the values of Refs. 7 and 11 as experimental values). We see that the difference of the calculated numbers with respect to the experimental ones is small. The largest discrepancy corresponds to the $1A_{1g} \rightarrow 2A_{1g}$ transition, due to the larger error, commented above, in the calculations of this transition in the chloride host.

The good agreement with the experimentally determined intraconfigurational transitions makes us confident about the positions of the higher lying and experimentally unresolved interconfigurational transitions. With these energies we can make fittings of the transition energies using ligand field parameters, including spin-orbit effects.[60,61] We have made these fittings using the energies of the intraconfigurational transitions and a number of low-lying interconfigurational ones, a total of 24 transition energies. The results of these fittings are $10Dq = 29\,948$ cm^{-1}, $B = 513$ cm^{-1}, $C = 1944$ cm^{-1}, and $\zeta = 3460$ cm^{-1} (fluoride cluster) and $10Dq = 25\,025$ cm^{-1}, $B = 445$ cm^{-1}, $C = 1313$ cm^{-1}, and $\zeta = 3089$ cm^{-1} (chloride cluster). The root-mean square deviations of these 24 level fittings are 227 cm^{-1} for the fluoride and 346 cm^{-1} for the chloride. It is clear from the fittings that both ligand field parameters $10Dq$ and spin-orbit parameters ζ are quite large for both systems. The parameters for the fluoride cluster are larger than for the chloride, as can be expected from ligand field arguments. These parameters can be compared with those found for $Os^{4+}:Cs_2GeF_6$ (Ref. 7) ($10Dq = 24\,570$ cm^{-1}, $B = 500$ cm^{-1}, $C = 4.76B = 2380$ cm^{-1}, and $\zeta = 3000$ cm^{-1}) and for $Os^{4+}:Cs_2ZrCl_6$

(Ref. 11) ($10Dq=22\,400\ cm^{-1}$, $B=500\ cm^{-1}$, $C=3B=1500\ cm^{-1}$, and $\zeta=2600\ cm^{-1}$). Our calculated values for $10Dq$ are appreciably larger than those obtained from experiments and the ζ as well. Our results are consistent with the experimentally based fittings performed for other $5d$ ions in fluoride coordination,[62] which result in $10Dq$ values of the order of $30\,000\ cm^{-1}$. It should be pointed out that the results of the fittings for d^4 ions rely heavily on the determination of interconfigurational transition energies and that the energy of these transitions has not been, as commented above, unambiguously determined in any experimental spectra. As a matter of fact, the fitting performed in Ref. 7 was done by assigning, quite arbitrarily, a weak absorption around $26\,000\ cm^{-1}$ to the $3\,T_{1g}$ state. This assignment is not supported by our calculations (see Table II). The fitting of Ref. 11 was done without any information about the interconfigurational levels and, due to that, their authors state that their calculated $10Dq$ values "are probably not precise."[11] We think that our calculated parameters should constitute a consistent set, useful for subsequent analyses of other systems.

Closely related to this fitting is the estimated position of the spin-orbit levels coming from the ^5E_g state. As this transition energy cannot be adequately determined experimentally, when its knowledge is necessary, it is estimated from ligand field calculations, using parameters obtained, as commented above, with very little and poor information about the $t_{2g}^3e_g^1$ levels. Using the parameters of the fitting commented above, Wermuth *et al.*[7] found that, for the fluoride system, the (^5E_g) states are located at around $16\,000\ cm^{-1}$, between the $2\,E_g$ and $2\,A_{1g}$ states, in a spectral region where no features are detected. According to these estimations, the t_{2g}^4 and $t_{2g}^3e_g^1$ manifolds of states overlap notably in Os^{4+}-doped Cs_2GeF_6. The results of our calculations definitely do not support this estimation. On the other hand, the fitting performed by Kozikowski and Kiederling[11] on the spectrum of Os^{4+}-doped Cs_2ZrCl_6 located the (^5E_g) states at $17\,400\ cm^{-1}$, just above the $2\,A_{1g}$ state. Again our results disagree in this point, as we predict a gap of around $3300\ cm^{-1}$ between these states. Taken together, those two estimates predict an increase (of around $1000\ cm^{-1}$) in the $1\,A_{1g}\rightarrow(^5E_g)$ transition energy due to chemical substitution (F–Cl), in sharp contrast with the trend found for the rest of the transitions (see Table V) and with our calculations, which predict a decrease of around $2000\ cm^{-1}$ for this transition energy.

The position of these (^5E_g) states has an important influence on the optical properties of the materials. Related to this and specially significant from our point of view is the lack of luminescence from the $2\,A_{1g}$ state in the fluoride cluster. In clear contrast with its chloride analog,[16] no luminescence has been detected from the $2\,A_{1g}$ state of Os^{4+}-doped Cs_2GeF_6, although different excitation energies have been tried.[5,7] The explanation of this fact has been related to the position of the lowest lying $t_{2g}^3e_g^1$ levels with respect of the $2\,A_{1g}$ state. In Ref. 5, Wermuth and Güdel suggested that some unidentified spin triplet state is very close (although higher) in energy to the $2\,A_{1g}$ state and the former can strongly couple to the lattice giving rise to a very efficient multiphonon relaxation that precludes luminescence from $2\,A_{1g}$. In Ref. 7, after locating the (^5E_g) states as commented above (around $16\,000\ cm^{-1}$), Wermuth *et al.* suggest that it is this (^5E_g) state that provides the way for nonradiative relaxation. From our calculations, we can offer an alternative explanation: it is the ^5E_g state that lies just above the intraconfigurational $2\,A_{1g}$ state and provides the necessary pathway to nonradiative relaxation. According to our calculations, the minimum-to-minimum energy difference between these two states is around $1500\ cm^{-1}$. Taking into account the calculated $\bar{\nu}_{a_{1g}}$ vibrational frequency (around $630\ cm^{-1}$, see Table II), this gap represent two to three of the largest vibrational energy quanta. We can see the crossing between both states in the large energy side of Fig. 2. This crossing is formally spin forbidden, however, the spin triplet character of the spin-orbit $2\,A_{1g}$ and $3\,A_{1g}$ states is, for all the distances studied here, of the order of 15%, so that the spin selection rule can be relaxed and this transition partially allowed by spin orbit. In this way, the lack of luminescence can be explained. Indeed, the same crossing exists in the chloride cluster but the energy difference between the relevant states is larger in this case, of around $3300\ cm^{-1}$ (i.e., around $9\bar{\nu}_{a_{1g}}$ vibrational energy quanta), and then, this mechanism is not competitive with the radiative relaxation from the $2\,A_{1g}$ state.

To sum up, our calculations show that the lowest energy region of the electronic structure of both $(OsF_6)^{2-}$ and $(OsCl_6)^{2-}$ embedded clusters consist of two separated manifolds, corresponding to the t_{2g}^4 and $t_{2g}^3e_g^1$ configurations. The differential effect of chemical substitution of the ligand (F–Cl) on the energy gap between these manifold is very considerable ($1500\ cm^{-1}$, $\simeq 2\bar{\nu}_{a_{1g}}$ for the fluoride; $3300\ cm^{-1}$, $\simeq 9\bar{\nu}_{a_{1g}}$ for the chloride) and is a key factor to understand the different behavior with respect to luminescence (both down-and up-converted luminescence) found in the title materials.

VI. CONCLUSIONS

In this work, we have presented *ab initio* calculations of the electronic structure of $(OsF_6)^{2-}$ and $(OsCl_6)^{2-}$ clusters embedded in Cs_2GeF_6 and Cs_2ZrCl_6, respectively, in order to determine the parameters relevant to the optical spectra of the materials. As a first step, the geometrical structure of the clusters is optimized, and we obtain equilibrium metal-ligand distances and a_{1g} vibrational frequencies. Our calculations show very reasonable agreement with the experimental data, mainly regarding the values of the totally symmetric a_{1g} vibrational frequencies and the positions of intraconfigurational electronic transitions. Reliable predictions about the location of states that are not easily accessible from the experiments can be made as well. The transition energies to states coming from the $t_{2g}^3e_g^1$ electron configuration have been determined this way. Assignments are proposed for several spectral features previously unassigned and some reassignments are discussed too. Using the calculated transition energies, we have performed fittings using ligand field parameters and found a consistent set of parameters from them.

As a result of the calculations we have found that the states related to the t_{2g}^4 and $t_{2g}^3e_g^1$ electron configurations of the Os^{4+} ion form two separate manifolds, without overlap

between them. The energy gap between them is quite sensitive to the nature of the ligand and the chemical substitution of F by Cl as ligand increases this gap from 1500 to 3300 cm^{-1}. In terms of the largest vibrational energy quanta, this gap amounts between two to three quanta (fluoride) and nine quanta (chloride). This result provides an alternative explanation to the lack of luminescence from the $2A_{1g}$ state in $Os^{4+}:Cs_2GeF_6$ based on the position of the ^5E_g spin-free state. On the other hand, our calculations also support the hypothesis of a relatively large energy gap between the $2T_{2g}$ and $2E_g$ states, of around 1000 cm^{-1}, which is somewhat controversial from the experimental point of view.

ACKNOWLEDGMENT

This work has been partly supported by MCyT (Dirección General de Investigación Project No. BQU2002-01316), Spain.

[1] D. R. Gamelin and H. U. Güdel, Top. Curr. Chem. **214**, 1 (2001).
[2] M. Wermuth and H. U. Güdel, Chem. Phys. Lett. **281**, 81 (1997).
[3] M. Wermuth and H. U. Güdel, J. Am. Chem. Soc. **121**, 10102 (1999).
[4] D. R. Gamelin, M. Wermuth, and H. U. Güdel, J. Lumin. **83–84**, 405 (1999).
[5] M. Wermuth and H. U. Güdel, J. Lumin. **87–89**, 1014 (2000).
[6] M. Wermuth and H. U. Güdel, J. Chem. Phys. **114**, 1393 (2001).
[7] M. Wermuth, C. Reber, and H. U. Güdel, Inorg. Chem. **40**, 3693 (2001).
[8] P. B. Dorain, H. H. Patterson, and P. C. Jordan, J. Chem. Phys. **49**, 3845 (1968).
[9] S. B. Piepho, J. R. Dickinson, J. A. Spencer, and P. N. Schatz, Mol. Phys. **24**, 609 (1972).
[10] S. M. Khan, H. H. Patterson, and H. Engstrom, Mol. Phys. **35**, 1623 (1978).
[11] B. A. Kozikowski and T. A. Kiederling, Mol. Phys. **40**, 477 (1980).
[12] A. R. Reinberg, Phys. Rev. B **3**, 41 (1971).
[13] G. C. Allen, R. Al-Mobarak, G. A. M. El-Sharkawy, and K. D. Warren, Inorg. Chem. **11**, 787 (1972).
[14] D. Durocher and P. B. Dorain, J. Chem. Phys. **61**, 1361 (1974).
[15] R. Wernicke, G. Eyring, and H.-H. Schmidtke, Chem. Phys. Lett. **58**, 267 (1978).
[16] C. D. Flint and A. G. Paulusz, Mol. Phys. **41**, 907 (1980).
[17] T. Schönherr, R. Wernicke, and H.-H. Schmidtke, Spectrochim. Acta, Part A **38**, 679 (1982).
[18] B. A. Kozikowski and T. A. Kiederling, J. Phys. Chem. **87**, 4630 (1983).
[19] L. A. Woodward and M. J. Ware, Spectrochim. Acta **20**, 711 (1964).
[20] K.-I. Ikeda and S. Maeda, Inorg. Chem. **17**, 2698 (1978).
[21] L. C. Weiss, P. J. McCarthy, J. P. Jasinski, and P. N. Schatz, Inorg. Chem. **17**, 2689 (1978).
[22] R. W. G. Wyckoff, *Crystal Structures*, 2nd ed. (Wiley, New York, 1965).
[23] R. McWeeny, Proc. R. Soc. London, Ser. A **253**, 242 (1959); Rev. Mod. Phys. **32**, 335 (1960); M. Kleiner and R. McWeeny, Chem. Phys. Lett. **19**, 476 (1973); R. McWeeny, *Methods of Molecular Quantum Mechanics* (Academic, London, 1989).
[24] S. Huzinaga and A. A. Cantu, J. Chem. Phys. **55**, 5543 (1971); S. Huzinaga, D. McWilliams, and A. A. Cantu, Adv. Quantum Chem. **7**, 187 (1973).
[25] Z. Barandiarán and L. Seijo, J. Chem. Phys. **89**, 5739 (1988).
[26] Z. Barandiarán and L. Seijo, in *Studies in Physical and Theoretical Chemistry: Computational Chemistry: Structure, Interactions, and Reactivity*, edited by S. Fraga (Elsevier, Amsterdam, 1992), Vol. 77(B), p. 435.
[27] J. L. Pascual and L. Seijo, J. Chem. Phys. **102**, 5368 (1995).
[28] B. G. Dick and A. W. Overhauser, Phys. Rev. **112**, 90 (1958).
[29] L. Seijo and Z. Barandiarán, in *Computational Chemistry: Reviews of Modern Trends*, edited by J. Leszczynski (World Scientific, Singapore, 1999), Vol. 4, p. 55.
[30] L. Seijo, Z. Barandiarán, and D. S. McClure, Int. J. Quantum Chem. **80**, 623 (2000).
[31] L. Seijo and Z. Barandiarán, J. Chem. Phys. **115**, 5554 (2001).
[32] H. M. Evjen, Phys. Rev. **39**, 675 (1932).
[33] Z. Barandiarán and L. Seijo, J. Chem. Phys. **115**, 7061 (2001).
[34] R. Llusar, M. Casarrubios, Z. Barandiarán, and L. Seijo, J. Chem. Phys. **105**, 5321 (1996).
[35] Z. Barandiarán and L. Seijo, J. Chem. Phys. **118**, 7439 (2003).
[36] L. Seijo and Z. Barandiarán, J. Chem. Phys. **118**, 5335 (2003).
[37] B. Ordejón, L. Seijo, and Z. Barandiarán, J. Chem. Phys. **119**, 6143 (2003).
[38] B. O. Roos, P. R. Taylor, and P. E. M. Siegbahn, Chem. Phys. **48**, 157 (1980); P. E. M. Siegbahn, A. Heiberg, J. Almlöf, and B. O. Roos, J. Chem. Phys. **74**, 2384 (1981); P. Siegbahn, A. Heiberg, B. Roos, and B. Levy, Phys. Scr. **21**, 323 (1980).
[39] K. Andersson, P.-Å. Malmqvist, B. O. Roos, A. J. Sadlej, and K. Wolinski, J. Phys. Chem. **94**, 5483 (1990); K. Andersson, P.-Å. Malmqvist, and B. O. Roos, J. Chem. Phys. **96**, 1218 (1992).
[40] A. Zaitsevskii and J. P. Malrieu, Chem. Phys. Lett. **233**, 597 (1995).
[41] J. Finley, P.-Å. Malmqvist, B. O. Roos, and L. Serrano-Andrés, Chem. Phys. Lett. **288**, 299 (1998).
[42] M. Casarrubios and L. Seijo, J. Chem. Phys. **110**, 784 (1999).
[43] R. D. Cowan and D. C. Griffin, J. Opt. Soc. Am. **66**, 1010 (1976).
[44] J. H. Wood and A. M. Boring, Phys. Rev. B **18**, 2701 (1978).
[45] L. Seijo, J. Chem. Phys. **102**, 8078 (1995).
[46] J. Andzelm, M. Klobukowsky, E. Radzio-Andzelm, Y. Sakai, and H. Tatewaki, *Gaussian Basis Sets for Molecular Calculations* (Elsevier, Amsterdam, 1984).
[47] S. Huzinaga, Z. Barandiarán, L. Seijo, and M. Klobukowsky, J. Chem. Phys. **86**, 2132 (1987).
[48] S. López-Moraza, J. L. Pascual, and Z. Barandiarán, J. Chem. Phys. **103**, 2117 (1995).
[49] Z. Barandiarán and L. Seijo, Can. J. Chem. **70**, 409 (1992).
[50] T. H. Dunning, Jr. and P. J. Hay, in *Modern Theoretical Chemistry*, edited by H. F. Schaeffer III (Plenum, New York, 1977).
[51] Detailed core and embedding AIMP data libraries in electronic format are available from the authors upon request or directly at the address http://www.uam.es/quimica/aimp/Data/AIMPLibs.html
[52] G. Karlström, R. Lindh, P.-Å. Malmqvist *et al.*, Comput. Mater. Sci. **28**, 222 (2003).
[53] R. M. Pitzer, COLUMBUS suite of programs (ARGOS, CNVRT, SCFPQ, LSTRN, CGDBG, and CIDBG); see A. H. H. Chang and R. M. Pitzer, J. Am. Chem. Soc. **111**, 2500 (1989), and references therein for a description. CNVRT and LSTRN have been adapted to handle ECPAIMP integrals by L. Seijo. CIDBG has been modified for spin-free-state-shifted spin-orbit CI calculations by M. Casarrubios.
[54] V. I. Azarov, A. J. J. Raassen, Y. N. Joshi, P. Uylings, and A. N. Ryabtsev, Phys. Scr. **56**, 325 (1997).
[55] G. Racah, Phys. Rev. **63**, 367 (1943).
[56] R. D. Shannon, Acta Crystallogr., Sect. A: Cryst. Phys., Diffr., Theor. Gen. Crystallogr. **32**, 751 (1976).
[57] S. L. Chodos, A. M. Black, and C. D. Flint, J. Chem. Phys. **65**, 4816 (1976).
[58] W. Preetz, D. Ruf, and D. Tensfeld, Z. Naturforsch. B **39**, 1100 (1984).
[59] M. Debeau and H. Poulet, Spectrochim. Acta, Part A **25**, 1553 (1969).
[60] S. Sugano, Y. Tanabe, and H. Kamimura, *Multiplets of Transition-Metal Ions in Crystal* (Academic, New York, 1970).
[61] K. A. Schroeder, J. Chem. Phys. **37**, 2553 (1962).
[62] G. C. Allen and K. D. Warren, Struct. Bonding (Berlin) **19**, 105 (1974).